NANOINDENTATION & TRIBOLOGICAL TESTS – SUITABLE TOOLS FOR MODELLING THE NANOSTRUCTURE OF SHEET NACRE

Philippe Stempflé and Olivier Pantalé
Laboratoire Génie de Production, Ecole Nationale d'Ingénieurs, 47 Avenue d'Azereix, 65016 Tarbes Cedex, France
philippe.stempfle@enit.fr

Richard Kouitat Njiwa
Laboratoire de Science et Génie des Surfaces, Ecole des Mines, Parc de Saurupt, 54042 Nancy Cedex, France

Marthe Rousseau and Evelyne Lopez
Muséum National d'Histoire Naturelle (UMR 5178 CNRS-MNHN), CP 26, 43 Rue Cuvier 75005 Paris, France

Xavier Bourrat
Institut des Sciences de la Terre d'Orléans, 1A Rue de la Férollerie, 45071 Orléans Cedex 2, France

1 Introduction

Nacre (the pearly internal layer of seashells) is a natural nanocomposite currently studied for the design of new organic/inorganic hybrid materials by mimicking biomineralization processes. It is a bioceramic formed at ambient temperature and pressure [1] which displays an exceptional high strength, stiffness and toughness [2] to weight ratio, as well as a natural biocompatibility with human bones [3].

These exceptional properties are generally ascribed to its highly ordered layered microstructure [4,5] described as a *"brick and mortar"* arrangement [6] where (Fig. 1): the *bricks* (97% in weight) refer to flat crystals of calcium carbonate ($CaCO_3$) in the crystalline form of aragonite (thickness less than 500 nm); and the *mortar* (3% in weight) refers to an "*intercrystalline"* thin network (about 40 nm) of a biological organic adhesive composed of silk-fibroin-like proteins and β-chitin [1-3]. In addition (Fig. 1c), each aragonite platelet consists of nanosized crystals of $CaCO_3$ surrounded by a water-soluble "*intracrystalline"* organic phase organised as a foam with very thin walls and closed porosity [7,8,9]. Thus, the platelet is itself a nanograin-reinforced organic matrix composite.

The aim of this paper is to understand some of the fracture mechanisms induced by friction as evidenced in a previous study [9]. First, spherical nanoindentation will enable to assess the elastic properties of each component of sheet nacre – *i.e* aragonite platelet and *intercrystalline* organic phases – by using either an experimental way or a numerical identification from a structural model. For this purpose, AFM analysis (Atomic Force Microscopy) is a suitable tool for characterizing and modelling the *multiscale* structure of nacre. Then, two structural models will be proposed for describing the respective structure of sheet nacre and that of the platelet.

Finally, two Finite Elements models – devoted respectively to quasi-static and dynamic loads – will be considered in order to support a new friction-induced fracture mechanism.

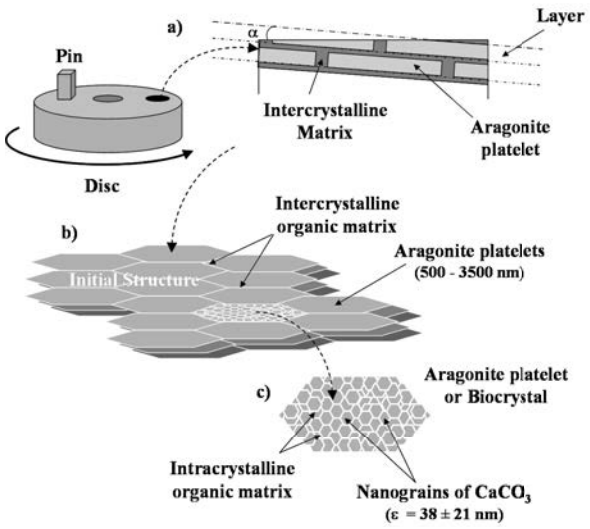

Figure 1: a) Schematic cross section of the friction surface. Multiscale structure of sheet nacre: b)aragonite platelets are surrounded by an "intercrystalline" organic matrix. c) Each platelet is constituted by nanosized $CaCO_3$ crystals (or nanograins) surrounded by an "intracrystalline" organic phase.

2 Experimental

2.1 Samples

Samples are made of sheet nacre extracted from giant oyster *Pinctada maxima* [9]. They are polished more or less parallel

to the aragonite platelets (Ra = 14.5 ± 0.6 nm). The average size of the initial nanograins as determined by AFM image analysis (Fig. 10) is 38 ± 21nm. The thickness of the "intracrystalline" matrix is about 4 nm.

2.2 Nanoindentation

The mechanical properties of samples are obtained with a *NHT nanoindenter* manufactured by *CSM Instruments*. It is composed of two elements: an instrumented nanoindenter and an optical microscope (enlargements, ×50 and ×1000). These elements are linked with an electromechanical positioning system (X,Y), which allows a relocation of the sample between the indenter and the microscope within a precision of 0.5µm. The vertical displacement and loading resolutions are, respectively, 0.03 nm and 1 µN. The compliance of the apparatus is 0.25 nm.mN^{-1}. A 5 µm radius spherical diamond indenter is used (E_i = 1141 GPa, ν_i = 0.07). Due to the specificities of material, the standard methods of analysis - *i.e* Oliver & Pharr [10], Field & Swain [11] - are not really suitable for determining the real Young's modulus. Thus, a *Hertzian* analytical solution is fitted onto the experimental curves in order to determine the Young's modulus and the yield stress. A minimum of 30 indentations is carried out for each test.

2.3 Tribological tests

We used a pin-on-disc tribotester manufactured by *CSM Instruments*. The tests are carried out at ambient air and room temperature in dry conditions by repeated friction of a 3.5 mm square shaped pin of nacre against the surface of a polished disc of nacre (∅ 44 mm). The normal load varies from 1 to 6 N corresponding to a mean contact pressure of 0.1 to 0.5 MPa. The speed and the distance of sliding are respectively 10 mm.s^{-1} and 100 m.

2.4 AFM & Image Analysis

Topography is assessed by using an Atomic Force Microscope *Dimension 3000* connected to an electronic controller: *Nanoscope IIIa* manufactured by *Digital Instruments (USA).* Its spatial and vertical resolutions are lower than 1 nm and the field depth in-between 100 nm and 100 µm. The micrographs were achieved in high resolution (512×512 pixels) by using an intermittent contact mode (*TappingMode™*) which minimizes the interactions between the probe and the surface during the acquisition and largely enhances the resolution compared to the contact-mode [12]. A *Phase Detection Imaging* (PDI) provides the *phase contrast* maps which improve the detection of the particles edges during the images analysis [13]. The silicon nitride probe is displaying a tip rounding lower than 10 nm. The work frequency, the stiffness and the cantilever amplitude are respectively: 270 kHz, 42 Nm^{-1} and 25nm.

According to the size of the images (between 0.25 and 25 µm^2), the scanning rate is varied from 1 to 2.4 µms^{-1}.

The size, the shape and the volume fraction of biocrystals nanograins were determined, from the *phase contrast* maps, with a specific algorithm integrated in the SPM data analysis software *Scanning Probe Image Processor* by *Image Metrology*. Analysis was made from cumulated measurements of at least 5,000 particles (images of 0.25 – 1µm^2).

3 Results and Discussion

3.1 Tribological Tests

In dry friction, the friction coefficient is rather high (µ=0.45), The wear coefficients *K* of the pin and the disc are reported in the table 1. They clearly reveal an important dissymmetry: the wear of the pin is negligible compared to the one of the disc. For that reason, we will be able to consider a rigid pin in the following numerical simulation.

	Pin	**Disc**
K (µg.m^{-1}.N^{-1})	1.418	32.602

Table 1: Wear coefficients K

Figure 2 shows a typical AFM view of the friction track after 100 m of sliding. After cleaning, it is observed that the worn surface of the disc is strongly degraded by parallel cracks which follow the structure of sheet nacre.

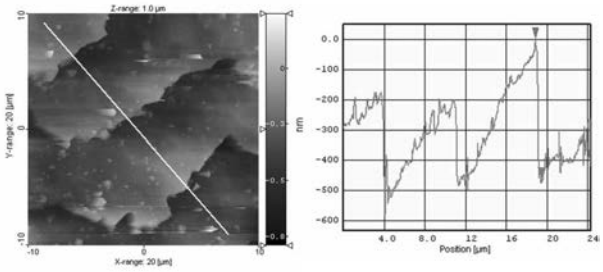

Figure 2: Typical AFM view (20× 20 µm^2) and topographic profile of the friction track

The morphology of these parallel cracks reveals two sorts of typical edge lines :

• On the one hand (Fig. 3), the crack is cut clear. The damage mechanism is clearly a brittle fracture around the aragonite platelets which involves the fracturing inside the *"intercrystalline"* organic matrix at the interface between adjacent platelets.

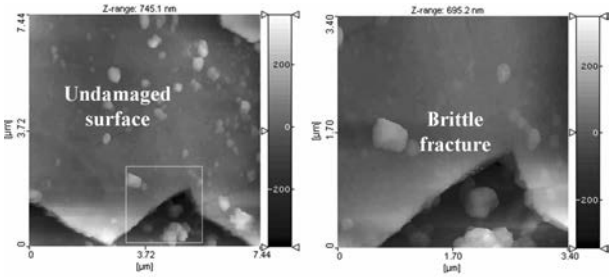

Figure 3:Typical AFM views of the morphology of the edge line in the case of the brittle fracture

• On the other hand (Fig. 4), the crack edges are rough and strongly disturbed. The damage is a kind of crumbling of the aragonite platelets. In this case, the fracture is supposed to occur inside the aragonite platelets itself and involves the fracturing of the *"intracrystalline"* organic matrix.

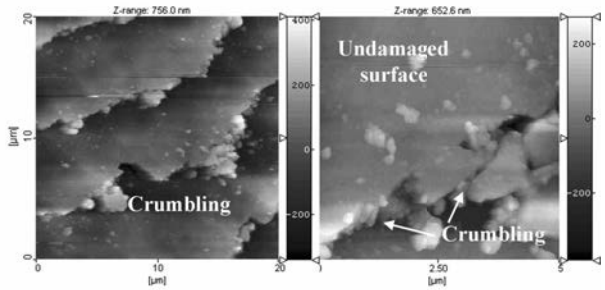

Figure 4: Typical AFM views of the morphology of the edge line in the case of crumbling

A thorough analysis of the various fracture mechanisms of sheet nacre, reported in the literature [2,4,5,14-22], reveals that they necessarily involve the *"intercrystalline"* organic matrix because it contributes to the energy absorption during crack propagation. Fragmentation of the aragonite platelets has never been reported in the literature. However, this damage is one of the main events observed in tribological testing [9]. Hence, the strength of the bonding at organic/inorganic interface appears to play an important role in the fracture mechanisms of nacre and thus in the wear mechanisms [18].

A Finite Elements Analysis should enable to understand this particular fracture mechanism induced by friction. The required mechanical parameters of nacre's components – *i.e* the aragonite platelet and the *"intercrystalline"* organic phase – are determined by nanoindentation.

3.2 Nanoindentation of aragonite platelets

Figure 5 shows the load-depth curves obtained with a 5µm radius indenter for 2 mN maximal load. The curves reveal a purely elastic behaviour of the aragonite platelets. As the curves are slightly disturbed, the standard analysis methods - like Oliver & Pharr or Field & Swain - are not really suitable. Hence, a *Hertzian* contact analytical solution was fitted onto the experimental curves in order to determine the Young's modulus (Fig. 6). The average value identified from the whole tests is : E = 62.49 ± 17.16 GPa.

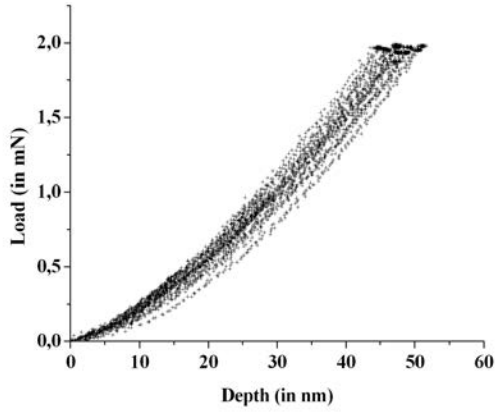

Figure 5 : Experimental load-depth curves performed on aragonite platelets at low loads

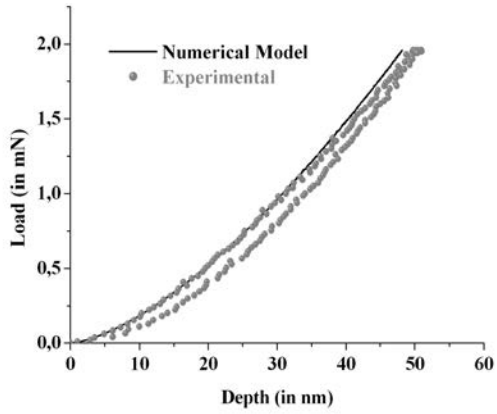

Figure 6: Typical load-depth curve and numerical Hertzian model allowing the identification of elastic mechanical properties of aragonite platelets

Figure 7 shows the load-depth curves obtained for 10 mN maximal load. At this load, a dissipative component is clearly observed under the load-depth curves. As shown in the insert (Fig. 7), the dissipative component corresponds to a plastic deformation involving piling-up phenomena. The previous *Hertzian* model enables to extract the limit of the elastic domain – *i.e* the compressive yield stress (about σ_y = 2 – 3 GPa);

In the tests where the load was pushed up to 20 mN, the contribution of the *"intercrystalline"* matrix was observed because the penetration depth becomes higher than 400nm. The Young's modulus decreased from 62.5 to 54.4 GPa, corresponding to the Young's modulus of sheet nacre – *i.e.*

aragonite platelets + *intercrystalline* organic phase (E = 54.42 ± 1.73 GPa).

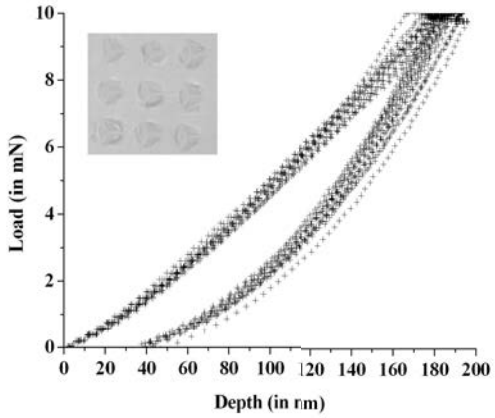

Figure 7: Experimental load-depth curves performed on aragonite platelets at high load. Insert: spherical imprints after tests.

3.3 Properties of the *intercrystalline* organic matrix

Knowing the mechanical properties of the aragonite platelets (62.5 GPa) and the nacre (54.4 GPa), the mechanical properties of the *"intercrystalline"* organic phase could be drawn from a structural model. According to Rousseau *et al.* [7,8], the *Pinctada maxima* sheet nacre does not present mineral bridges between the platelets. The *"intercrystalline"* matrix is continuous.

Hence, in first approximation (Fig. 8), it can be considered that the spherical nanoindentation at high loads gives the transversal Young's modulus (E_T) of a stacking of layers made up of pure matrix and reinforced layers (mineral and organic).

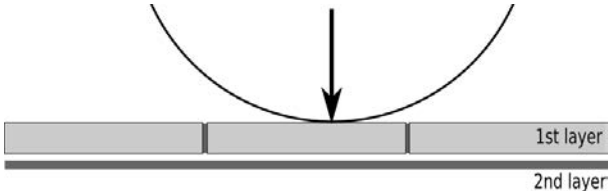

Figure 8: Illustration of the model used for identifying elastic properties of the intercrystalline matrix (dark grey) vs. those of the platelet (light grey)

This transversal Young's modulus is given by the relation [23] :

$$E_T = \left(\frac{1}{E_f - E_m\left(1 - \frac{1}{\sqrt{V_f}}\right)} + \frac{1-\sqrt{V_f}}{E_m} \right)^{-1}$$

where E_f, and E_m are respectively the Young's modulus of the aragonite platelets and the *"intercrystalline"* organic matrix. V_f is the volume fraction of the platelets, considering nacre as a composite of platelets and *"intercrystalline"* organic matrix. This relation provides a good approximation of the Young's modulus of the matrix (E_m) as a function of E_f and E_T, determined by nanoindentation respectively using low and high loads.

Results show that the *"intercrystalline"* organic matrix Young's modulus is 10 times lower than the one of the aragonite platelets (Table 2).

E_T (GPa)	E_f (GPa)	V_f	E_m (GPa)
54.424	62.489	0.97	**6.308**

Table 2: Identified Young's modulus of the intercrystalline organic matrix

Knowing the mechanical properties of the constitutive components of sheet nacre, a Finite Elements Model is now used to illustrate the specific fracture processes induced by friction.

3.4 Numerical simulations

Many attempts have been conducted, in the last past years, to simulate the mechanical behaviour of sheet nacre [4, 24-27]. One of the major conclusions, deduced from those simulations, is that the fracture of the sample usually occurs inside of the biological *"intercrystalline"* organic matrix as reported for example by Ji *et al*. [4].

But, according to the knowledge of the authors, the structure is only subjected to quasi-static monotonic loading in tension in all those simulations. From a preliminary look at the identified component elastic properties reported in Table 3, the mechanical properties of the aragonite platelet [A] are higher than the one of the biological *"intercrystalline"* organic matrix [M].

	E (GPa)	σ_y (GPa)	ν	ε^{max}
[A]	62.5	2	0.2	1%
[M]	6.3	0.116	0.3	10%

Table 3: Identified mechanical properties

Comparison of material properties leads to conclude that, in quasi-static traction tests, high shear region and crack propagation may only be located inside of the organic matrix. However, tribological tests have shown that the main fracture phenomenon occurs inside of the aragonite platelet. The main difference between the tribological test and quasi-static tests (tension, compression, bending…) is the presence of repeated shocks induced by dynamic effects. The aim of the two numerical models presented below is to show the effect of these shocks on the localization of the fracture.

3.4.1 Numerical models used for FEM simulations

The first numerical model is used to simulate a quasi-static compression test and the second one to simulate the impact of a rigid body on a sheet nacre specimen. The Abaqus Explicit FEM code [28] is used to solve both problems. Figure 9 shows the main characteristics of the models used for simulation. The inclination angle of 8° between the impactor trajectory and the platelets has been evaluated using the AFM facility. Material mechanical properties used in both simulations are compiled in Table 3. From one model to the other one, only the boundary conditions linked to the rigid impactor vary.

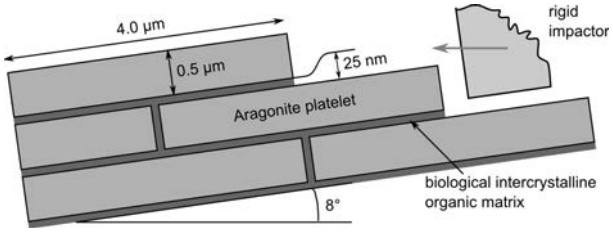

Figure 9: Model used for numerical simulation

In order to simulate the fracture inside both materials, a ductile damage law is used in this simulation based on the maximal strain values (ε^{max}) reported in Table 3. For the aragonite platelet, the plastic deformation is probably controlled by the *"intracrystalline"* organic matrix surrounding the $CaCO_3$ grains (fig 10). Therefore, the maximal strain value of the platelet is estimated from the volume fraction of the organic matrix within the platelet, estimated by AFM image analysis (about 12% in 2D corresponding to 4.2% in 3D).

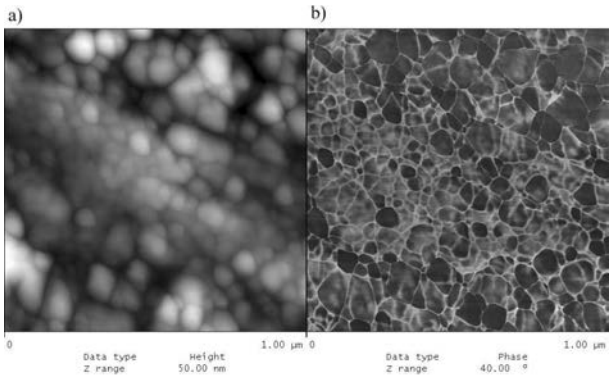

Figure 10: Typical AFM views of the polished surface of an aragonite platelet observed in tapping-mode: topographic (a) and phase contrast maps revealing the nanosized grains of $CaCO_3$ surrounded by the intracrystalline organic matrix .

Within this approach, when the ductile damage criterion is reached, the corresponding element is considered completely damaged, and is removed from the FE model using the erosion algorithm of the Abaqus code. In both numerical simulations, the rigid impactor is moved with a prescribed velocity of 10 $mm.s^{-1}$ – corresponding to the relative tribological test velocity. Contact is assumed to be frictionless.

3.4.2 Quasi-static compression test

In this first application, the initial contact length between the aragonite platelet and the rigid impactor is 50 nm – *i.e.* 10% of the total platelet height. An initial velocity equal to the impactor velocity has been applied on all nodes of the platelet in order to suppress the shock component at the beginning of the simulation. The velocity direction is parallel to the aragonite platelets arrangement. Figure 11 shows the *von Mises* contourplot for a total displacement d = 30 nm of the rigid impactor.

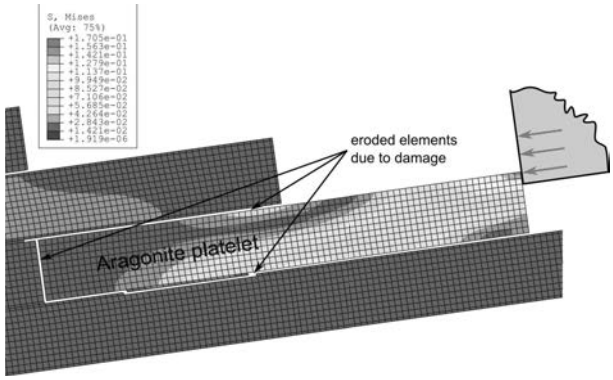

Figure 11: Results for the quasi-static compression test

Numerical results show that the *"intercrystalline"* organic matrix is completely fractured, as reported by other authors [4] using quasi-static traction or bending tests, while the aragonite platelet remains intact after deformation and becomes free. Fracture lines within the nacre sheet are clearly represented by the use of the erosion algorithm coupled with the damage law.

3.4.3 Dynamic impact test

In this second application, the initial contact length between the aragonite platelet and the impactor is also 50 nm. This approach is similar to one used in a previous work for the numerical simulation of a machining process proposed by Pantalé *et al.* [29]. The main difference is that the workpiece is built with a composite material. Figure 12 shows the *von Mises* stress contourplot for a total horizontal displacement d = 125 nm of the impactor after the first contact.

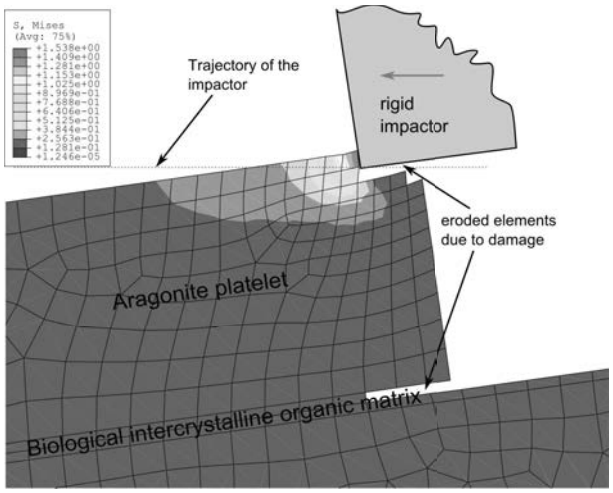

Figure 12: Numerical results for the impact test

Numerical results show some highly concentrated stresses in the vicinity of the contact zone between the impactor and the platelet as reported in machining operations. As a main consequence of dynamic effects, and the presence of repeated shocks, the fracture zone reported in Figure 12 is totally different from the one reported in Figure 11. Major part of the fracture is now located inside of the aragonite platelet, in accordance with experimental observations using tribological tests. Stresses distribution, reported in Figure 12, show that during the impact, the ratio between the equivalent stress and the yield stress ($\overline{\sigma}/\sigma_y$), inside the biological *"intercrystalline"* organic matrix, is lower than the one inside of the platelet.

Therefore, fracture propagation inside the organic matrix is limited (intercrystalline). Different simulations have shown that the ratio between the number of fractured elements inside of the platelet and inside of the organic matrix increases when the height of the contact zone decreases – *i.e* when the shearing depth decreases. This usually occurs in tribological tests.

3.5 Mechanical properties of the components of the aragonite platelets

Although many works were carried out to elucidate the mechanical behaviour of nacre [2, 4, 5, 14-22, 24-27], no approach has been made to link it to the nanomechanical properties of the elemental components constituting the aragonite platelets – i.e biocrystals and "*intracrystalline"* organic phase.

Previous results showed that nanoindentation provides a good estimation of the aragonite platelets mechanical properties whereas tribological testing enables the assessment of their nanostructure by considering the morphology of the fracture edge line (Fig. 13).

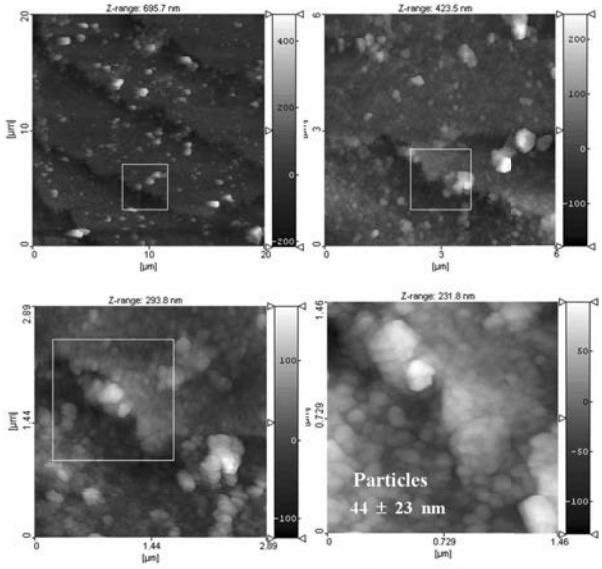

Figure 13: Typical AFM views of crumbled edge lines (successive enlargements) showing the structure of the aragonite platelets.

As shown in fig. 10 – structure before sliding – and the various enlargements (Fig. 13) achieved on the edge of the crack after platelets crumbling, the platelets can be considered like a $CaCO_3$ nanoparticles-reinforced organic composite material, where the volume fraction of each component can be assessed by AFM image analysis.

Figure 10 confirms that the structure of the *"intracrystalline"* matrix is continuous around the nanograins [7,8]. Hence, one can consider the platelets like a composite material where mineral nanoballs are drowned into a continuous organic matrix. Each phase being homogeneous, the elastic properties of this composite can be determined by the Mori-Tanaka model [30] given by the following relations :

$$k_c = k_m + \frac{V_r k_m (k_r - k_m)}{k_m + (1-V_r)\alpha_m (k_r - k_m)}$$

$$\mu_c = \mu_m + \frac{V_r \mu_m (\mu_r - \mu_m)}{\mu_m + (1-V_r)\beta_m (\mu_r - \mu_m)}$$

with

$$\alpha_m = \frac{3k_m}{3k_m + 4\mu_m}, \quad \beta_m = \frac{6(k_m + 2\mu_m)}{5(3k_m + 4\mu_m)}$$

and

$$k_i = \frac{E_i}{3(1-2\nu_i)}, \quad \mu_i = \frac{E_i}{2(1+\nu_i)} \quad (i = m, r, c)$$

Where V_r is the volume fraction of nanograins. Details and complete hypotheses are available in [31].

An hypothesis about the Poisson's ratio of the *"intracrystalline"* organic phase is considered in this work (ν = 0.29). From the identified mechanical properties of the platelets, the numerical simulation of the above model provides respectively the Young's modulus of the *"intracrystalline"* organic matrix and the Poisson's ratio of the nanograins (Table 4).

	E (GPa)	ν (GPa)
Platelet	62.5	0.2
Aragonite nanograin	96 [a)]	**0.17**
Intracrystalline organic matrix	**3.6**	0.29

[a)] assessed by Berkovich nanoindentation

Table 4: Identification of the mechanical properties of the aragonite platelets components (i.e. aragonite grains and intracrystalline organic matrix)

These results show that the *"intracrystalline"* organic matrix is almost 2 times less rigid than the *"intercrystalline"* organic matrix (Table 2). These results should enable to explain the elastoplastic behaviour of the aragonite platelets observed in nanoindentation.

4 Conclusions

The aim of this work was to understand the fracture mechanisms induced by friction with an approach combining tribological tests, experimental charac-terization and numerical simulation for quasi-static and dynamic loads. Results show that :

• Spherical nanoindentation provides a good approximation of the platelets mechanical properties whereas tribological testing enables to study their nanostructure – *i.e* shape, size and arrangement of aragonite nanograins within the biocrystal;

• From raw results of nanoindentation, the identification of the mechanical properties of the aragonite platelets components is possible by using various *"multiscale"* structural models. This way, the identified elastic properties of the *"intracrystalline"* organic matrix was found to be about 2 times lower than that of the *"intercrystalline"* one. This explains the purely elastic behaviour of the platelet at low loads;

.• The comparison of Finite Elements models built respectively for quasi-static and dynamic loads provides enlightenment on the fracture mechanism induced by friction. It shows that this latter is linked to dynamic effects, which have a significant influence on performances and fracture location.

5 Acknowledgements

The authors wish to thank C. Poigneau from SIERA SA for having supplied them with the nacre samples.

6 References

[1] S. Weiner, L. Addadi, *J. Mater., Chem.,* (1997), 7, (5), 689-702 ;
[2] K. Okumura, P. G. de Gennes, *Eur. Phys. J.,* E 4, (2001), 121-127 ;
[3] P. Westbroek, F. Mari, *Nature,* Vol. 392, (1998), 861-862;
[4] B. Ji, H. Gao, *J. Mech. Phys. Solids*, (2004), 52, 1963-1990 ;
[5] N.M. Neves, J. F. Mano, *Mater. Sci. and Engineer.: C*, 25, 2, (2005),113-118;
[6] L. Addadi, S. Weiner, *Nature,* (1997), 389, 912-913;
[7] M. Rousseau, E. Lopez, Ph. Stempflé, M. Brendlé, L. Franke, A. Guette, R. Naslain, X. Bourrat, *Biomaterials,* 26, 31, (2005), 6254 - 6262;
[8] M. Rousseau, X. Bourrat, Ph. Stempflé, M. Brendlé, E. Lopez, *Key Engi. Mater.*Vols. 284 -286 (2005), pp 705-708 ;
[9] Ph. Stempflé, M. Brendlé, *Tribology International*, 39, (2006), 1485-1496;
[10]W.C. Oliver, G. M. Pharr*, J. Mater. Res.,* 7, 4, (1992), 1564-1583;
[11]J. S. Field, M. V. Swain, *J. Mater. Res.,* 8, 2, (1993), 297-306;
[12]J. P. Aimé, R. Boigard, L. Nony, G. Couturier, *J. Chem. Phys* (2001), 114, 11, 4945-4954 ;
[13]S. N. Magonov, V. Elings, M-H. Wangbo, *Surf. Sci.* (1997), 375, (2-3), L385-391;
[14]A.P. Jackson et al, *Compos. Sci. Tech.* (1989), 36, 255-266;
[15]A.P. Jackson et al, *J. Mater. Sci. Lett.,* (1986), 5, 975-978 ;
[16]M. Sarikaya et al, *Mater., Res. Soc. Symp. Proc.,* (1990), 174, 109-131 ;
[17]R. Z. Wang et al, *J. Mater. Sci.,* (1995), 30, 2299-2304 ;
[18]B.L. Smith et al, *Nature,* (1999), 399, 761-763 ;
[19]S.P. Kotha et al, *J. Mater. Sci,* (2001), 36, 2001-2007 ;
[20]K. Okumura, *Eur. Phys. J. E,* (2002), 7, 303-310 ;
[21]R. Z. Wang et al, *J. Mater. Res.* (2001), 16, 9, 2485-2493;
[22]A. G. Evans et al, *J. Mater. Res.* (2001), 16, 9, 2475-2484 ;
[23]D. Gay, *Matériaux composites*, Hermes Lavoisier, ISBN 2-7462-1098-3 (2005), 670p ;
[24]J. Wu et al, *J. Biomech,* (1998), 31, 165-169 ;
[25]D.R. Katti, K. S. Katti, *J. Mater. Sci.,* (2001), 36, 1411-1417;
[26]D.R. Katti et al, *Comput. Theor. Polym. Sci.* (2001), 11, 397-404;
[27]P.K.V.V. Nukala, S. Simunovic, *Biomaterials,* (2005), 26, 6087-6098;
[28] K. Hibbitt, I. Sorensen, *Abaqus Theory Manual*, HKS, (1997) ;
[29]O. Pantalé et al. *Comp. Meth. App. Mech. Eng*. (2004), 193 (39/41), 4383-4399 ;
[30]T. Mori, K. Tanaka, *Acta Metal*. (1973), 21,571;
[31]Y. Benveniste, *Mechanics of Materials,* vol. 6, (1987), pp. 147-157 ;